Progress in Propulsion Physics **11** (2019) 543-554
https://doi.org/10.1051/eucass/201911543

PARAMETRICAL STUDY ON SIDE LOAD GENERATION IN SUBSCALE ROCKET NOZZLES

R. Stark and C. Génin

German Aerospace Center
Langer Grund, Lampoldshausen 74239, Germany

The flow separation within convergent–divergent rocket engine nozzles induces undesired side loads. As the flow separation cannot be avoided during startup and shutdown processes of the engine, the understanding of the resulting side loads is of crucial interest. To develop and validate side load models, an experimental parametrical study was conducted. The parameters of interest were the length of the separated backflow region, the wall contour angle, and the total pressure gradient during startup and shutdown processes. For this reason, three subscale models were designed and tested in five configurations. As the main side load driver, a comparably slow moving separation front, passing a long and narrow backflow region, could be identified.

1 INTRODUCTION

The flow within a convergent–divergent rocket nozzle can only achieve a certain degree of overexpansion. Beyond, the boundary layer lifts off the nozzle wall and ambient air is sucked into the remaining separated backflow section of the nozzle. For a given nozzle geometry, the position of the flow separation is a function of gas properties and total and ambient pressure. The prediction of the separation position is crucial for rocket engine design as it determines the maximum possible nozzle area ratio, a deciding factor for the engine performance. Nevertheless, during startup and shutdown, the total pressure of the engine changes leading to flow separation within the divergent nozzle section. With increasing total pressure, the flow separation is shifted downstream towards the nozzle exit until the engine operational condition with a full flowing nozzle is achieved.

The flow separation is asymmetrically distributed in circumferential direction and the resulting wall pressure differences on opposite sides of the nozzle induce undesired side loads. These side loads that cannot be avoided stress the

© The Authors, published by EDP Sciences. This is an open access article distributed under the terms of the Creative Commons Attribution License 4.0 (http://creativecommons.org/licenses/by/4.0/).

Article available at https://www.eucass-proceedings.eu or https://doi.org/10.1051/eucass/201911543

nozzle, the rocket engine, the engine actuators, the launcher structure, and the payload. For this reason, it is of interest to model and to predict the side loads induced by flow separation. Successful side load prediction models will enable lighter nozzles, thrust chambers, and actuators. Especially, a reduced load transmission will profit the future application of lightweight electrical driven engine actuators.

To generate side load model validation data, DLR performed the tests with three subscale nozzles under various conditions. The aim was to study the influence of parameters like length of separated backflow region or nozzle wall contour angle on side load generation. A special attention was put on the total pressure gradient as this might be a deciding factor for modeling and comparison of the nozzles of different sizes.

2 EXPERIMENTAL SETUP

The parametrical study was conducted at DLR's cold flow subscale test facility P6.2 in Lampoldshausen. Figure 1 gives a sketch of the facility assembly with its 20-megapascal high-pressure gaseous nitrogen supply storage. The line system includes automatic valves, filters, pressure reducers, regulation valves, and mass

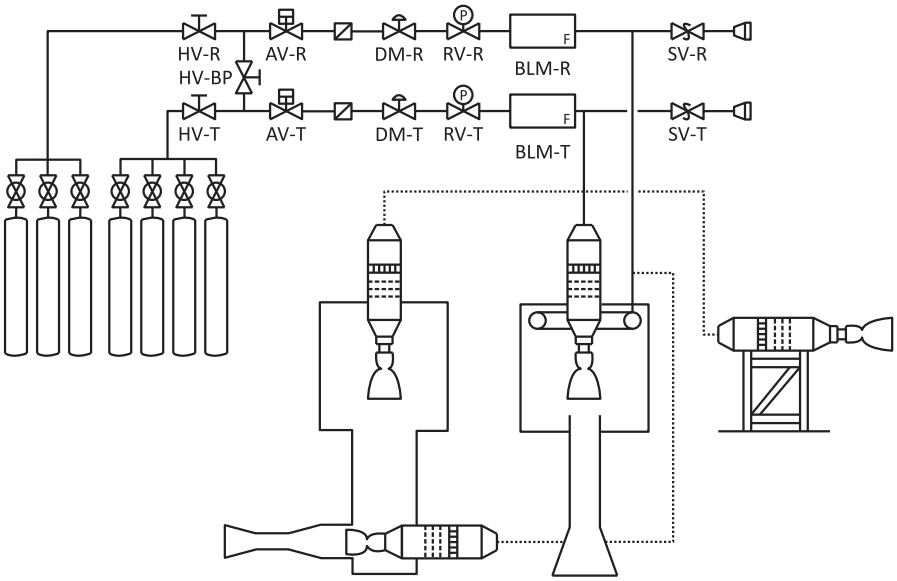

Figure 1 Sketch of facility assembly P6.2

flow meters. It connects the supply storage with the settling chambers, mounted vertically at the top of the high-altitude chamber (middle) or horizontally at the test rig (right). A third facility setup offers an additional ejector system to decouple the high-altitude chamber pressure from the test specimen throughput (left). To reduce turbulence, the settling chambers are equipped with a set of grids and honeycombs. The presented study was performed under ambient conditions using the horizontal test rig.

Test facility P6.2 features total pressures up to 6 MPa and mass flows up to 4.2 kg/s. Dry gaseous nitrogen is used as working fluid to avoid condensation effects (H_2O, CO_2, O_2, etc.). The nitrogen total temperature corresponds to ambience.

2.1 Nozzle Design

For the purpose of this study, three truncated ideal contour (TIC) nozzles have been designed. The nozzles feature design Mach numbers of $\mathrm{Ma}_D = 4.8$, 5.3, and 5.8. They are designated as TIC-2048, TIC-2053, and TIC-2058. The nozzles share the same subsonic geometry with a throat radius of $R_{\mathrm{th}} = 10$ mm. Each of them was truncated to a length allowing full flowing condition at a nozzle pressure ratio of $\mathrm{NPR} = p_0/p_a = 50$, leading to identical wall exit pressures with a wall exit Mach number of $\mathrm{Ma}_e = 4.25$. The specimens were made of acrylic glass with a wall thickness of 8 mm. The main nozzle design parameters are given in Table 1.

One of the main factors of side load generation seems to be the inflow of ambient air into the separated backflow region. Hence, it was foreseen to truncate nozzle TIC-2048 twice to obtain nozzles being full flowing for a NPR of 40 and 30 (Fig. 2*a*). With the resulting five configurations, it was possible to study the impact of the length of the separated backflow region and the wall contour angle as well.

Table 1 Design parameters of TIC nozzles

Nozzle	Design Mach number Ma_D	Exit wall Mach number Ma_e	Divergent length L_d $(1/R_{\mathrm{th}})$	Exit wall angle α_e	Area ratio $\varepsilon = A_e/A_{\mathrm{th}}$
TIC-2048	4.8	4.25/4.0/3.75[a]	13.9/10.7/8.1	4.9°/7.5°/10.1°	17.0/14.4/11.6
TIC-2053	5.3	4.25	11.7	8.4°	18.5
TIC-2058	5.8	4.25	10.3	11.3°	19.0

[a] Initial design / first truncation / second truncation.

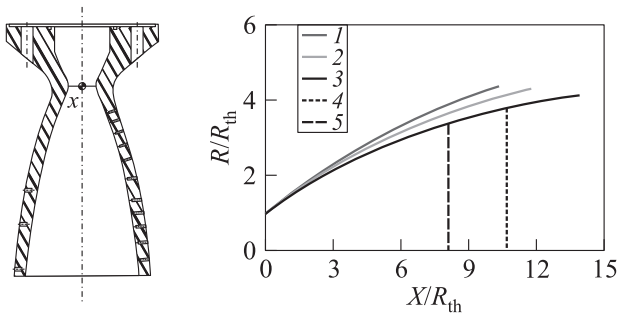

(*a*) (*b*)

Figure 2 Sketch of TIC-2048 (*a*) and designed nozzle wall contours (*b*): *1* — $M_d = 5.8$; *2* — 5.3; *3* — 4.8; *4* — 4.8, Cut 1; and *5* — $M_d = 4.8$, Cut 2

2.2 Pressure and Side Load Measurement

The nozzles were equipped with two axial rows of pressure ports. One row featured a constant axial spacing of 4 mm. Depending on the nozzle configuration, 16 to 30 ports could be implemented. The second row was radially shifted with 90° (Fig. 3*a*). Its port arrangement reproduces the wall Mach number progress. The resulting data are more suitable for a statistical validation of wall Mach number based separation criteria [1].

The static wall pressures were measured via 0.5-millimeter orifices drilled perpendicular into the nozzle wall. These orifices were connected with small metal pipes and Teflon tubes to collecting blocks where piezoresistive Kulite XT-154-

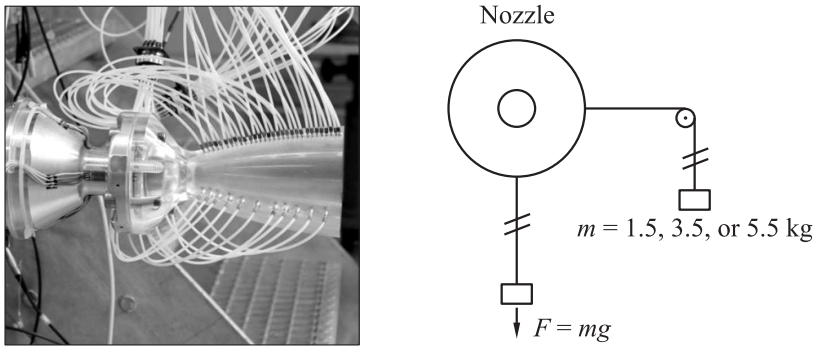

(*a*) (*b*)

Figure 3 Mounted TIC-2048 (*a*) and side load calibration method (*b*)

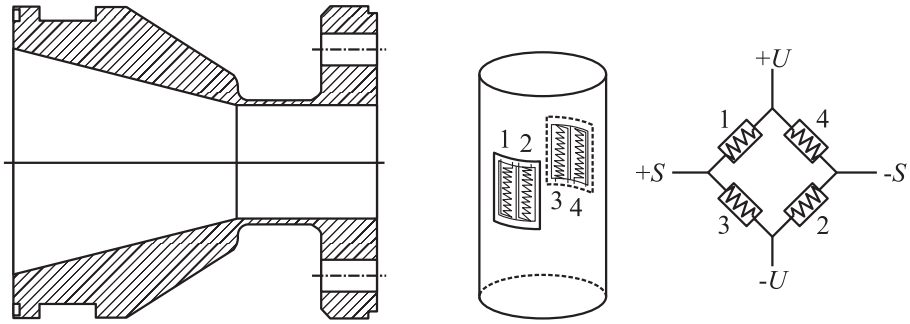

(*a*) (*b*)

Figure 4 Sketch of bending tube (*a*) and strain gauges application (*b*)

190M absolute pressure transducers were screwed into. The transducers had a measurement range of 1 bar with an accuracy of 0.5% relative to the upper range limit. The natural frequency of the transducers pressure sensitive semiconductor membrane is higher than 50 kHz but, due to the low eigenfrequency of the Teflon tubes, the pressure signals were filtered with a cutoff frequency of 160 Hz and recorded with a frequency rate of 1 kHz. Three selected port signals were recorded with a high frequency of 25 kHz.

The side loads were measured simultaneously using a thin walled bending tube mounted upstream the subsonic nozzle inflow (see Figs. 3*a* and 4*a*). The contraction ratio between bending tube and nozzle throat was four. An asymmetric pressure distribution inside the nozzle causes a force perpendicular to the nozzle symmetry axis that consequently bends the tube. The resulting bending stresses on the surface of the tube are proportional to the induced load and are measured with HMB type 6/350 DY13 strain gauges. The strain gauges are arranged as pairs on opposite sides of the bending tube and connected as a full Wheatstone bridge. The wiring connects opposite branches of the bridge (see Fig. 4*b*). This kind of wiring assures that tensile, torsional, and temperature stresses are compensated and do not affect the bending measurement. Two full Wheatstone bridges were 90 degree radial shifted to detect the horizontal as well as the vertical side load component.

The setup was calibrated with different weights acting at the nozzle exit plane. The weights were applied with a string and releasing the weight by cutting its string (see Fig. 3*b*) gives the static as well as the dynamic response of the system. With this calibration, all measured voltage signals can be interpreted as loads acting at the end of the nozzle.

Figure 5*a* gives a calibration example where a force of 54 N is applied at the exit of nozzle TIC-2053. After release of the weight, the vibration char-

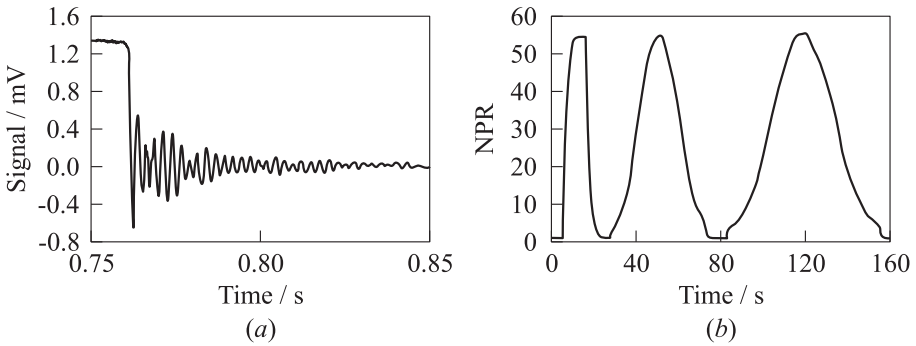

Figure 5 Example of a calibration signal (a) and test sequence TIC-2048, Run 08 (b)

acteristic of the bending tube appears with a damped beat frequency. The dominant frequency is 390 Hz and the superposed frequency is 300 Hz. All bending data were recorded with a frequency of 25 kHz using a signal filter of 8 kHz.

2.3 Test Sequence

Figure 5b depicts the NPR sequence used to test all five nozzle configurations. Three successive up- and down-ramping NPR gradients were realized: 25, 4.5, and 1.5 s^{-1}, respectively. In total, 47 tests were performed (Table 2). As all nozzles were tested with this common test sequence, the resulting side load measurements can be compared easily.

Table 2 Performed number of tests

Nozzle	Number of tests
TIC-2048	16
TIC-2048, first truncation	6
TIC-2048, second truncation	9
TIC-2053	9
TIC-2058	7

3 RESULTS AND DISCUSSION

Three parameters were studied: the length of the separated backflow region, the wall contour angle, and the NPR gradient. Figure 6 gives a representative side

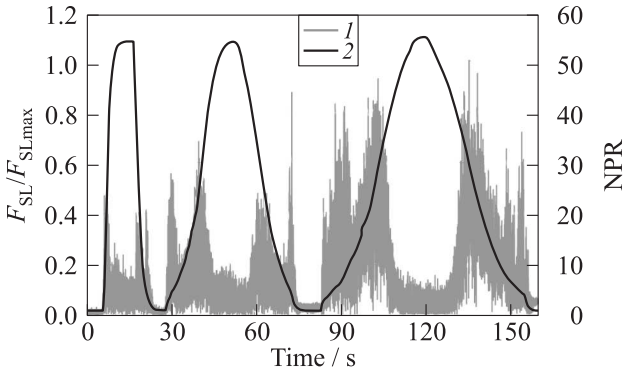

Figure 6 Side load progress (*1*) and NPR (*2*)

load measurement for the initial TIC-2048 nozzle. It appears that the side loads increase with decreasing NPR gradient. The side load data are standardized by the maximum side load peak occurred in Test 481, Run 8. All following side load charts are standardized by this value as well; so, a direct comparison is given.

Figure 7 illustrates the same side loads as a function of the NPR gradients, both for up- (Fig. 7*a*) and down-ramping (Fig. 7*b*) processes. The mean side load values appear to be lower for the down-ramping process, whereas the appearances of the peak values are comparable. Two distinct conditions with increased side loads are visible. The first one appears for a NPR below 10. Here, the boundary layer relaminarizes within the throat section due to the flow acceleration as a function of the local viscosity. In consequence, a laminar flow separation de-

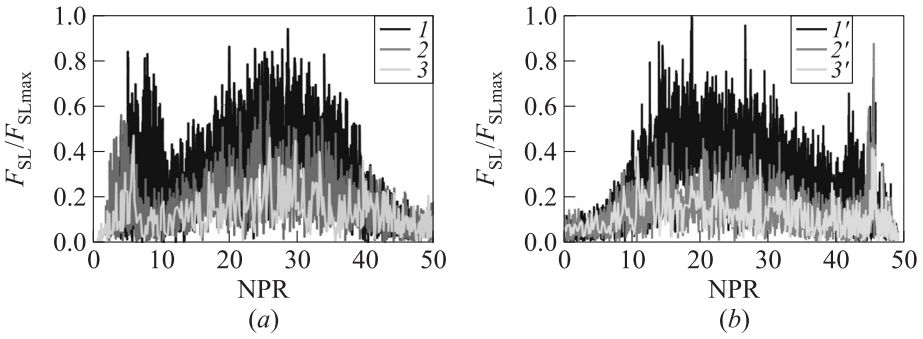

Figure 7 Side loads as functions of NPR gradient for up- (*a*) and down-ramping (*b*) processes: *1* — 1.5 s^{-1}; *1′* — −1.5; *2* — 4.5; *2′* — −4.5; *3* — 25; and *3′* — −25 s^{-1}

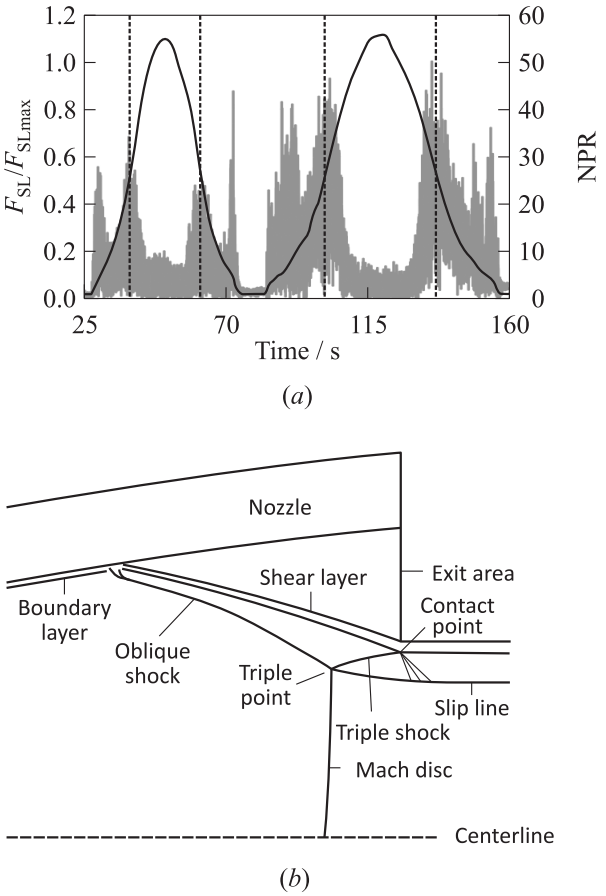

Figure 8 Side load maxima (a) and sketch of flow condition (b)

velops downstream the nozzle throat. With increasing NPR, the flow separation is shifted downstream towards the nozzle exit. As the local Reynolds number increases along the nozzle wall, at a certain point, a retransition to a turbulent boundary layer takes place. The turbulent flow separation is known to withstand higher pressure differences; so, the flow separation is immediately shifted downstream. As the retransition process is circumferentially inhomogeneously distributed, the resulting shock system of oblique separation shocks and Mach disc is tilted. The tilted Mach disc redirects the flow towards the wall where it reattaches partially. The resulting pressure differences on opposite side of the walls result in side loads [1, 2]. This stable flow state is called partial restricted flow separation, pRSS.

The characteristic of the second side load increase is illustrated as a function of NPR in Fig. 8*a*. Its occurrence is independent from the NPR gradient. Within this flow state, the so-called contact point crosses the nozzle exit plane (Fig. 8*b*). The contact point marks the position where the conical shaped shear layer is deflected by the reflected triple shock into a more cylindrical shape. Its position is directly linked to the origin of the oblique separation shock and the Mach disc position. As the separation position fluctuates, the contact point position moves likewise.

The exhaust jet fills a part of the nozzle exit cross section. The remaining exit area allows the backflow of ambient air into the separated nozzle section. Disturbances of the backflow directly interact with the flow separation into a closed regulation loop.

If the contact point fluctuates within the exit plane, the section is at times filled with a cylindrical shaped and at other times with a conical shaped shear layer. The diameter of the cylindrical shear layer nearly does not change. Consequently, there is a minor effect on the remaining exit area that is available for the backflow. The conical shear layer affects the remaining backflow area much more. The instantaneous change from a cylindrical to a conical shear layer therefore intensifies the backflow disturbances and the separation fluctuation is stimulated. As a consequence, the side loads increase. Considering this self-enhancing loop, it is obvious that an increased NPR gradient, which accelerates the downstream movement of the separation position, damps the side load generation as the nozzle exit transit time is reduced. In reverse, for stationary or quasi-stationary flow conditions (low NPR gradient), side loads might be intensified to an unrepresentative value that might not be useful for model validation or, at least, this flow state might have to be considered within modeling.

3.1 Length of Separated Backflow Region

Figure 9 compares representative side loads of the successively truncated TIC-2048. The truncation positions can be found in Fig. 2*b* and Table 1. It emerges that the truncation of the nozzle reduces the side loads. The impact of NPR gradient disappears and the peak value caused by pRSS decreases as the lever arm of the reattached flow is reduced. The NPR of the peak's appearance does not change either. The relaminarization is a function of the throat geometry and the gas properties, parameters that do not change.

The second side load maximum, caused by the fluctuating contact point, is shifted to lower NPRs. This is an expected result. The nozzle exit is relocated upstream and the contact point crosses it for lower NPR.

The successively truncated nozzles show almost no impact of the NPR gradient. It implies that the intensification of the backflow disturbances at low NPR gradients does not appear. This might be caused by the separation related

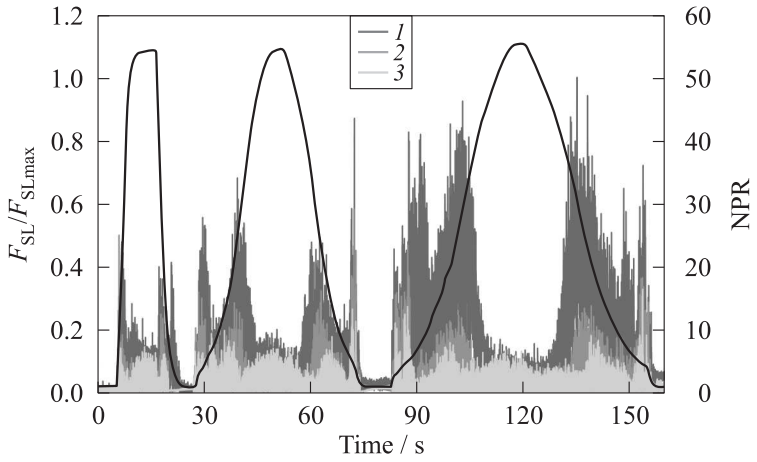

Figure 9 Side loads of initial TIC-2048 (*1*) and after the first (*2*) and the second (*3*) truncations

wall contour angle. An increased wall angle goes ahead with an increased wall Mach number gradient. Hence, the length of the separation zone with its fluctuating shock position is decreased in axial direction and the fluctuation of the linked contact point is reduced as well. The backflow disturbances are no longer intensified in a distinct quality.

3.2 Wall Angle Impact

Figure 10 presents a comparison of TIC-2048, TIC-2053, and TIC-2058. The side loads decrease with increasing design Mach number. Likewise, the effect of NPR gradient reduces. However, the overall side loads are still above the values of the truncated TIC-2048.

As mentioned, the flow separation fluctuates less in axial direction if the related wall angle is steeper. As a consequence, the closed loop of separation, exhaust jet, and backflow is less activated. On the contrary, low wall angles narrow the backflow region and the feedback effect induced by the exhaust jet gains influence. It is noticeable that the trend detected for the truncated TIC-2048, where the maximum side load is shifted for each additional truncation towards a lower NPR, reverses and the maximum side loads are shifted to a higher NPR with increasing design Mach number. This effect is particular noticeable for the lowest NPR gradient.

The ratios of NPR for the full flowing nozzle (see subsection 2.2) and related mean contact point transit $\mathrm{NPR_{FF}}/\mathrm{NPR_{trans}}$ yield for all five configurations

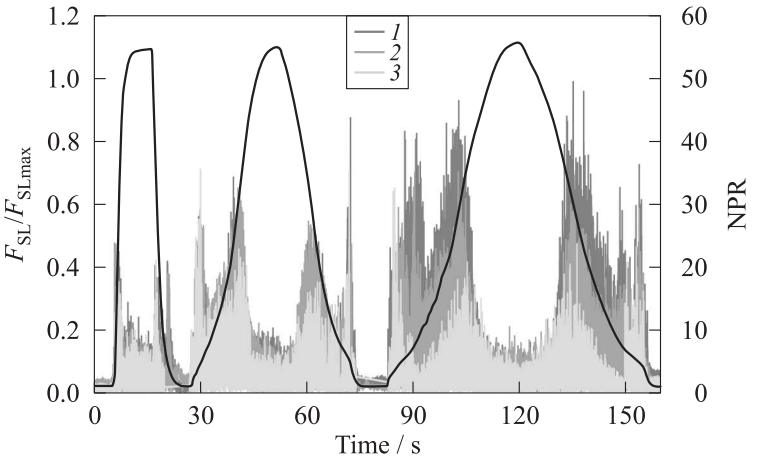

Figure 10 Side load comparison of TIC-2048 (*1*), TIC-2053 (*2*), and TIC-2058 (*3*)

Table 3 Measured side loads

	Side load, N		NPR_{FF}/NPR_{trans}
	Maximum	Mean	
TIC-2048	65–97	15–25	1.7
TIC-2048, first truncation	55–65	9	1.6
TIC-2048, second truncation	48	8	1.8
TIC-2053	60–80	15–25	1.6
TIC-2058	60–75	10–12	1.7

comparable values of 1.6–1.8 (Table 3). This correlation might ease the modeling and will be in focus for future studies.

4 CONCLUDING REMARKS

The tests were conducted to study the impact of the separated backflow region length, the wall contour angle, and the NPR gradient on side load generation. It appears that a slow moving separation front, passing a long and narrow backflow region, causes strongly increased side loads. As this slow movement is not the case for real rocket engine applications, such quasi-stationary validation configurations should be avoided or, at least, the slow NPR gradient should be included in modeling. Hence, as the main side load driver by design, the nozzle exit wall angle can be identified.

ACKNOWLEDGMENTS

The authors like to thank Dr. Manuel Frey, Thomas Aichner, and Dr. Adam Garus (all Airbus Safran Launchers GmbH) for fruitful cooperation within the framework of the German National Research Initiative Propulsion 2020.

REFERENCES

1. Stark, R., and B. Wagner. 2009. Experimental study of boundary layer separation in truncated ideal contour nozzles. *Shock Waves* 19(3):185–191.
2. Stark, R. 2010. Beitrag zum Verständnis der Strömungsablösung in Raketendüsen [Contribution to the understanding of flow separation in rocket nozzles]. RWTH Aachen, Germany. PhD Thesis.